

Supplementary Information

Atomically Well-defined Nitrogen Doping in the Cross-plane Transport through Graphene Heterojunctions

Hewei Zhang,^{‡a} Ping Zhou,^{‡b} Abdalghani Daaoub,^{‡c} Sara Sangtarash,^c Shiqiang Zhao,^a Zixian Yang,^a Yu Zhou,^a Yu-Ling Zou,^a Silvio Decurtins,^b Robert Häner,^b Yang Yang,^{*a} Hatef Sadeghi,^{*c} Shi-Xia Liu^{*b} and Wenjing Hong^{*a}

^a State Key Laboratory of Physical Chemistry of Solid Surfaces, College of Chemistry and Chemical Engineering & Pen-Tung Sah Institute of Micro-Nano Science and Technology, Xiamen University, 361005 Xiamen, China.

^b Department of Chemistry, Biochemistry and Pharmaceutical Sciences, University of Bern, Freiestrasse 3, 3012 Bern, Switzerland

^c Device Modelling Group, School of Engineering, University of Warwick, Coventry CV4 7AL, United Kingdom

[‡] These authors contributed equally to this work

* Corresponding author

Email: yangyang@xmu.edu.cn (Y. Y.); Hatef.Sadeghi@warwick.ac.uk (H. S.); shi-xia.liu@unibe.ch (S. L.); whong@xmu.edu.cn (W. H.)

Contents

1. Cross-plane break junction (XPBJ) setup.....	3
2. Graphene-based single-molecule junction measurement	4
3. Transition voltage spectrum.....	8
4. Ultraviolet photoelectron spectrum	9
5. UV-Vis spectrum	11
6. Computational methods.....	12
7. Supplementary computational figures, tables and discussion.....	14
8. Gold-based single-molecule junction measurement.....	18

1. Cross-plane break junction (XPBJ) setup

In order to fabricate Gr-molecule-Gr single-molecule junctions, we modified the scanning tunneling microscopy break junction (STM-BJ) setup used for gold electrode testing in the group to obtain the cross-plane break junction (XPBJ) setup. The Au tip was replaced with Cu wire with high-quality graphene on the surface made by chemical vapor deposition (CVD), and the Au substrate was replaced with Cu foil with graphene.

Photos of the specific XPBJ setup are shown in Figure S1.

We used the O-ring and liquid cell made of acid-resistant materials in order to fix the position of Cu foil, ensure its flatness and alleviate the volatilization of solvent. The Cu wire is bent into an O shape and loaded into the syringe as a tip and fixed onto the piezo stack. The stepper motor above the piezo enables the tip to move quickly over a wide range. A large number of nanogaps with different intervals can be rapidly fabricated between the tip and the substrate by piezo, and the adjustment range is 0~10 V. The copper/graphene composites involved in the tip and substrate were purchased from Six-Carbon Technology Shenzhen. 30~40 μL of solution were dripped in the liquid cell. The liquid cell was connected to the skeleton through magnets, making the tip to dip into the solution. A current amplifier and a controller were connected to the tip and the substrate, and the measurement is completed through our own developed program. During the break junction processes, a bias voltage of 100 mV was applied, and the current and voltage were recorded in real time at a sampling frequency of 20 kHz

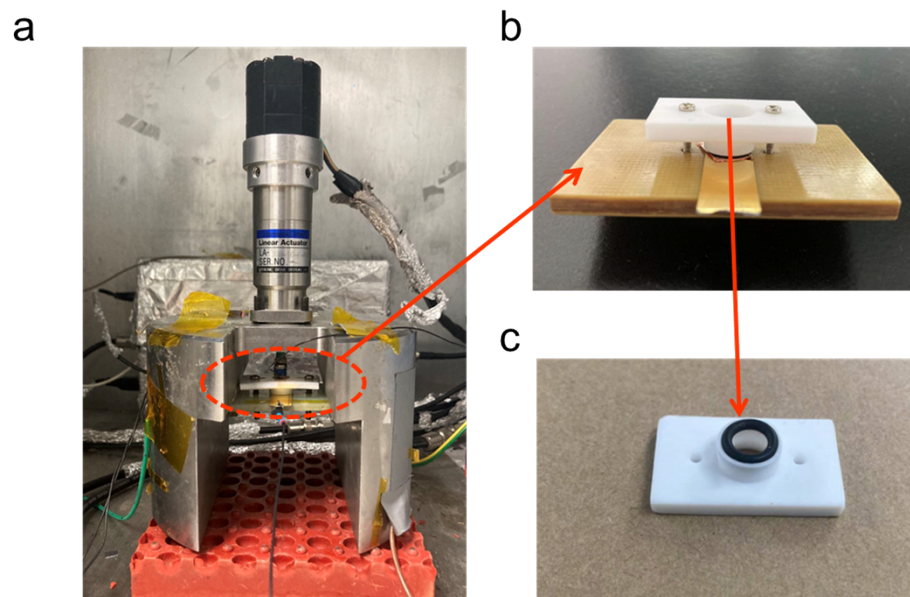


Fig. S1. The photos of the home-built XPBJ setup. (a) The photos of the whole installation. (b) The liquid cell installation. (c) The O ring and liquid cell.

In this work, iDSpec ARCTIC (NCS Testing Technology, Beijing) performed the Raman measurement. A confocal spectrometer with a $\times 50$ objective, a 632.8 nm excitation and a 600 lines/mm grating was used for all characterization. All data were obtained with an integration time of 5 s and a 4.96 mW laser power.

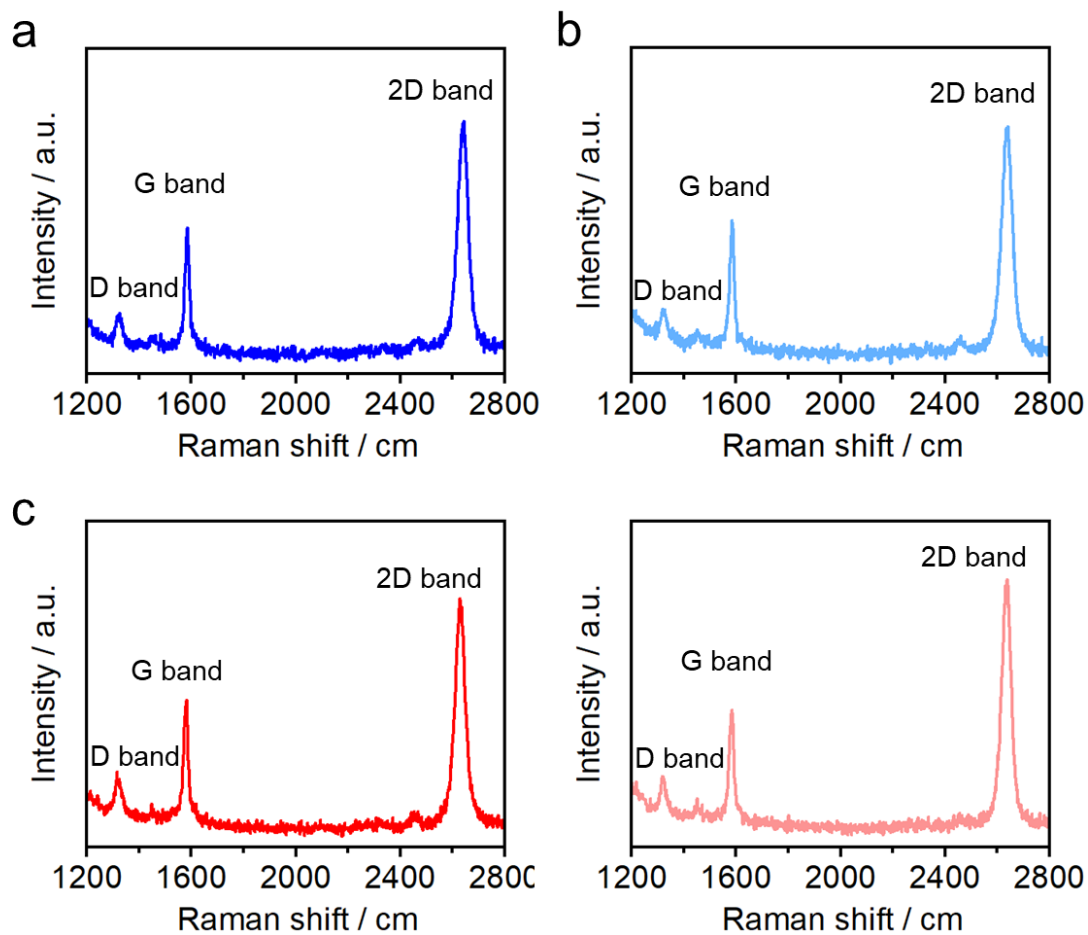


Fig. S2. Raman spectra of the graphene tip before break junction experiments (a), graphene tip after break junction experiments (b), graphene substrate before break junction experiments (c), and graphene substrate after break junction experiments (d).

2. Graphene-based single-molecule junction measurement

More than 1000 conductance traces were recorded during the measurement. When the conductance value is $10^{-3.0} G_0$, the individual traces are considered to reach zero¹⁻². We measured the electrical properties of the pure solvent decane, as shown in Figure S3. Conductance-displacement traces plummeted, 1D conductance histograms showed no pronounced peak, and 2D conductance-distance histograms showed no apparent plateau. Direct tunneling in the pure solvent is proved. The plateau length histograms were carried out for the conductance data from $10^{-3.0} G_0$ to $10^{-6.0} G_0$, and it was found that the plateau length of pure solvent decane was 0.27nm^{2-3} , which was consistent with the previous work report. The plateau lengths of other molecules were corrected on this basis.

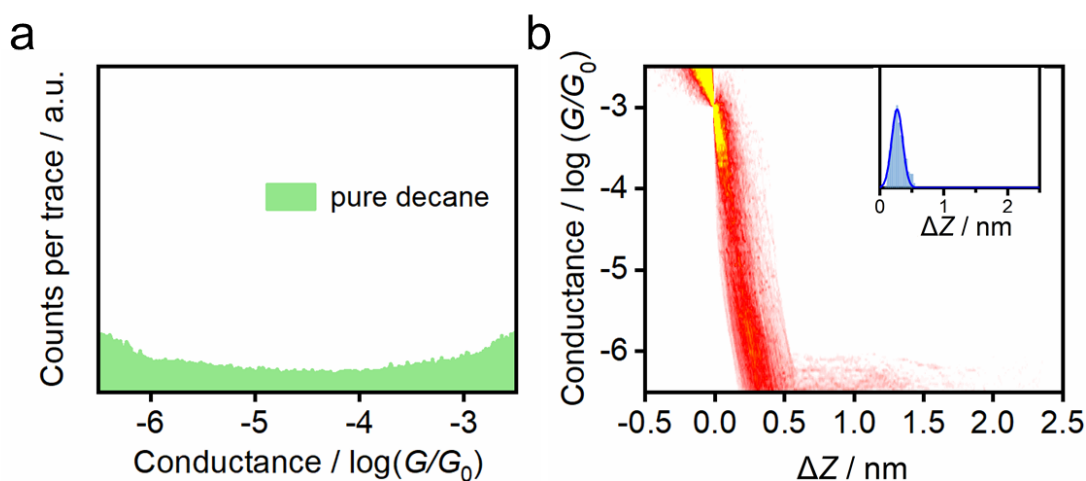


Fig. S3. Pure solvent measurement. (a) 1D conductance histogram and (b) 2D conductance versus plateau length histogram of the pure decane.

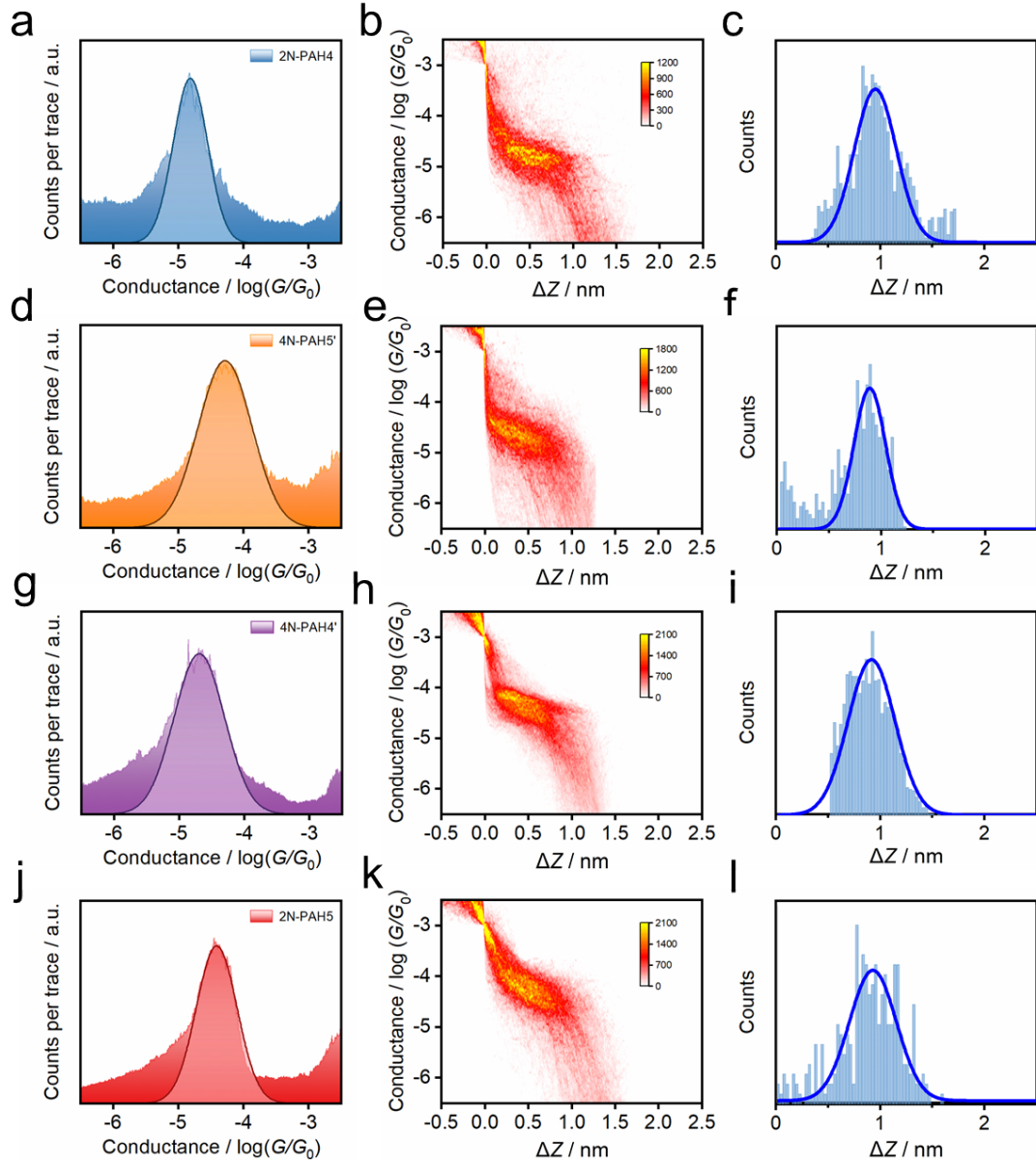


Fig. S4. Results of single-molecule conductance by XPBJ measurement. 1D conductance histograms of 2N-PAH4 (a), 2N-PAH5 (d), 4N-PAH4' (g), 4N-PAH5' (j). 2D conductance-distance histograms of 2N-PAH4 (b), 2N-PAH5 (e), 4N-PAH4' (h), 4N-PAH5' (k). The plateau length histograms of 2N-PAH4 (c), 2N-PAH5 (f), 4N-PAH4' (i), 4N-PAH5' (l).

Supplementary Table S1. Conductance difference -

Molecule	G / nS	G (N-PAH)/ G(PAH)
2N-PAH5	3.02	0.468
PAH5	6.45	
2N-PAH4	1.20	0.631
PAH4	1.90	
4N-PAH5'	4.07	0.794
PAH5'	5.12	
4N-PAH4'	1.58	1.35
PAH4'	1.17	

The biggest conductance difference due to different doping number of nitrogen atoms:

$$1.35 \div 0.468 = 288\%$$

The conductance difference due to nitrogen-doping at different positions in the conjugated framework:

$$1.35 \div 0.794 = 170\%$$

$$0.631 \div 0.468 = 135\%$$

3. Transition voltage spectrum

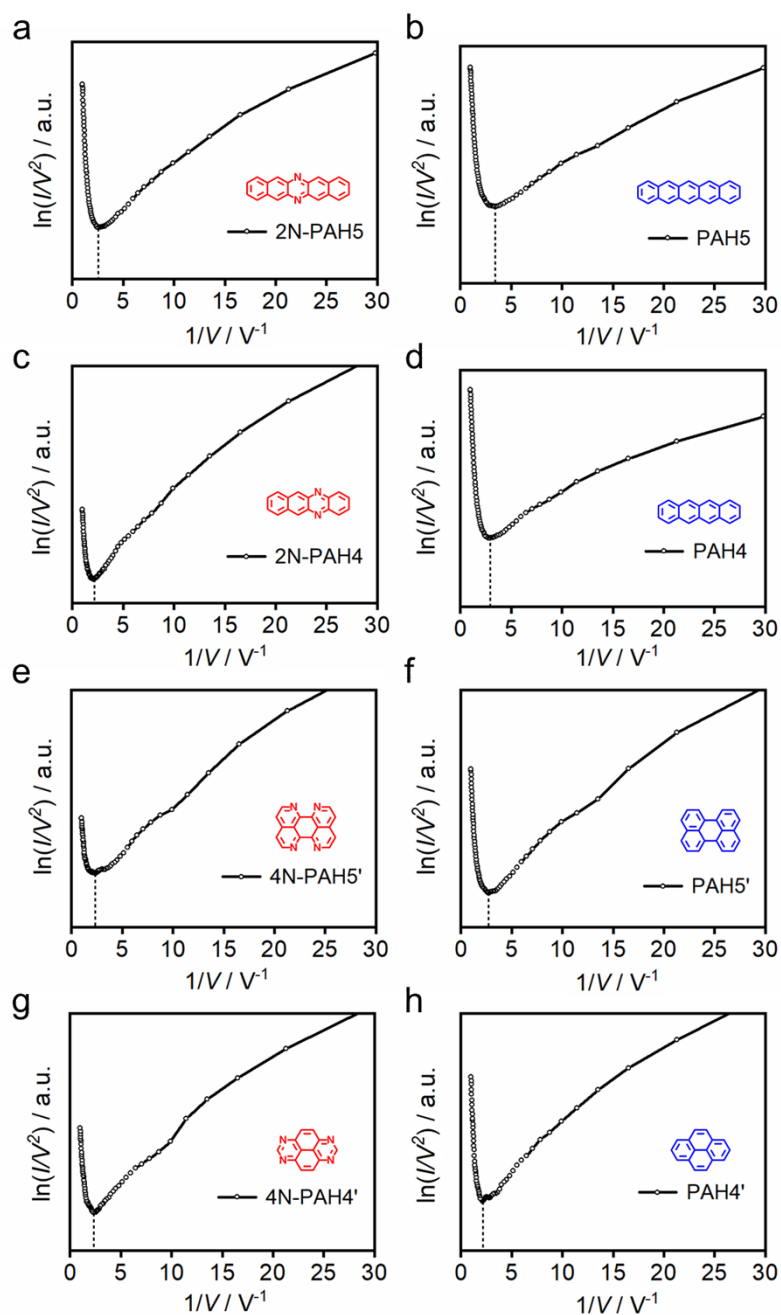


Fig. S5. Transition voltage ($\ln(I/V^2)$ vs $1/V$) spectra obtained from ~ 1000 I - V traces of 2N-PAH5 (a), PAH5 (b), 2N-PAH4 (c), PAH4 (d), 4N-PAH5' (e), PAH5' (f), 4N-PAH4' (g) and PAH4' (h).

4. Ultraviolet photoelectron spectrum

The electronic structure of N-PAHs and PAHs on copper foil with single-layer graphene was measured by UPS. All data were obtained using a HeI light source ($h\nu = 21.22$ eV) with a bias of -5 V applied to the sample. The Fermi energy level of the electrode was corrected with the gold electrode on the same bench, and the intensity was normalized.

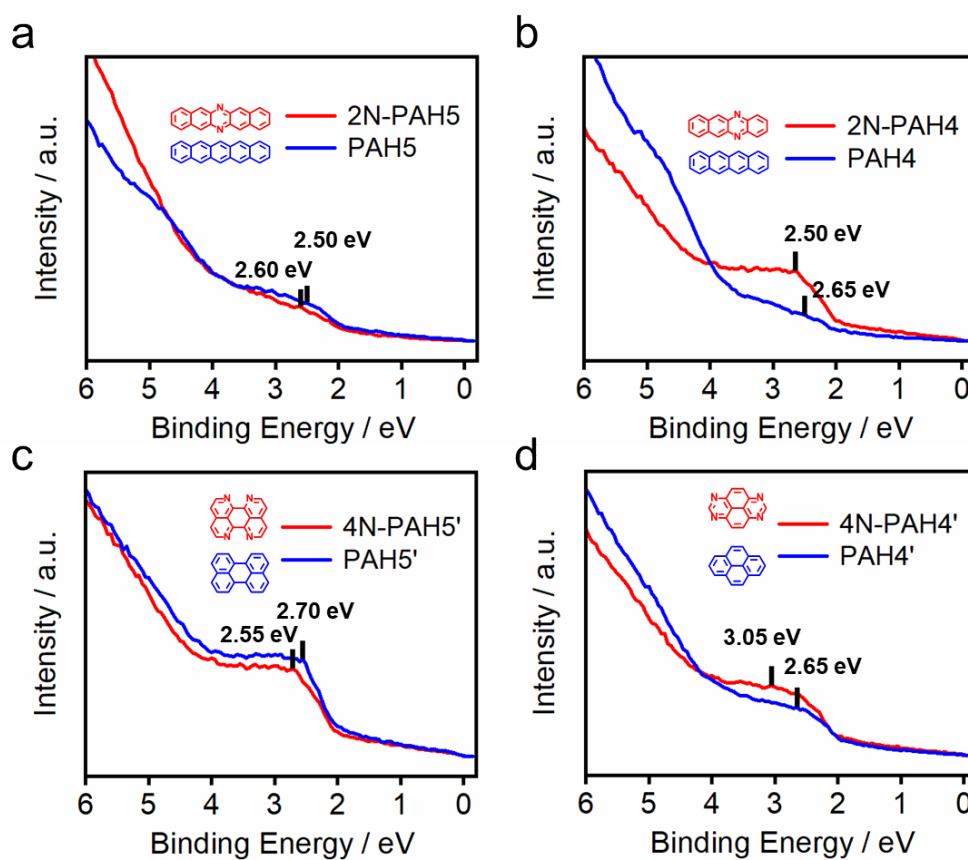


Fig. S6. Ultraviolet photoelectron spectra of 2N-PAH5 and PAH5 (a), 2N-PAH4 and PAH4 (b), 4N-PAH5' and PAH5' (c), 4N-PAH4' and PAH4' (d).

Supplementary Table S2. $E_F - E_{\text{HOMO}}$ of N-PAHs and PAHs by UPS

N-PAH	2N-PAH5	2N-PAH4	4N-PAH5'	4N-PAH4'
$E_F - E_{\text{HOMO}} / \text{eV}$	2.60	2.65	2.70	3.05
PAH	PAH5	PAH4	PAH5'	PAH4'

$E_F-E_{\text{HOMO}} / \text{eV}$	2.50	2.50	2.55	2.65
-----------------------------------	------	------	------	------

5. UV-Vis spectrum

According to an empirical formula:

$$E_g = 1240/\lambda_{\text{abs}}$$

E_g estimated from the UV-Vis spectrum onset of the lowest energy absorption band.

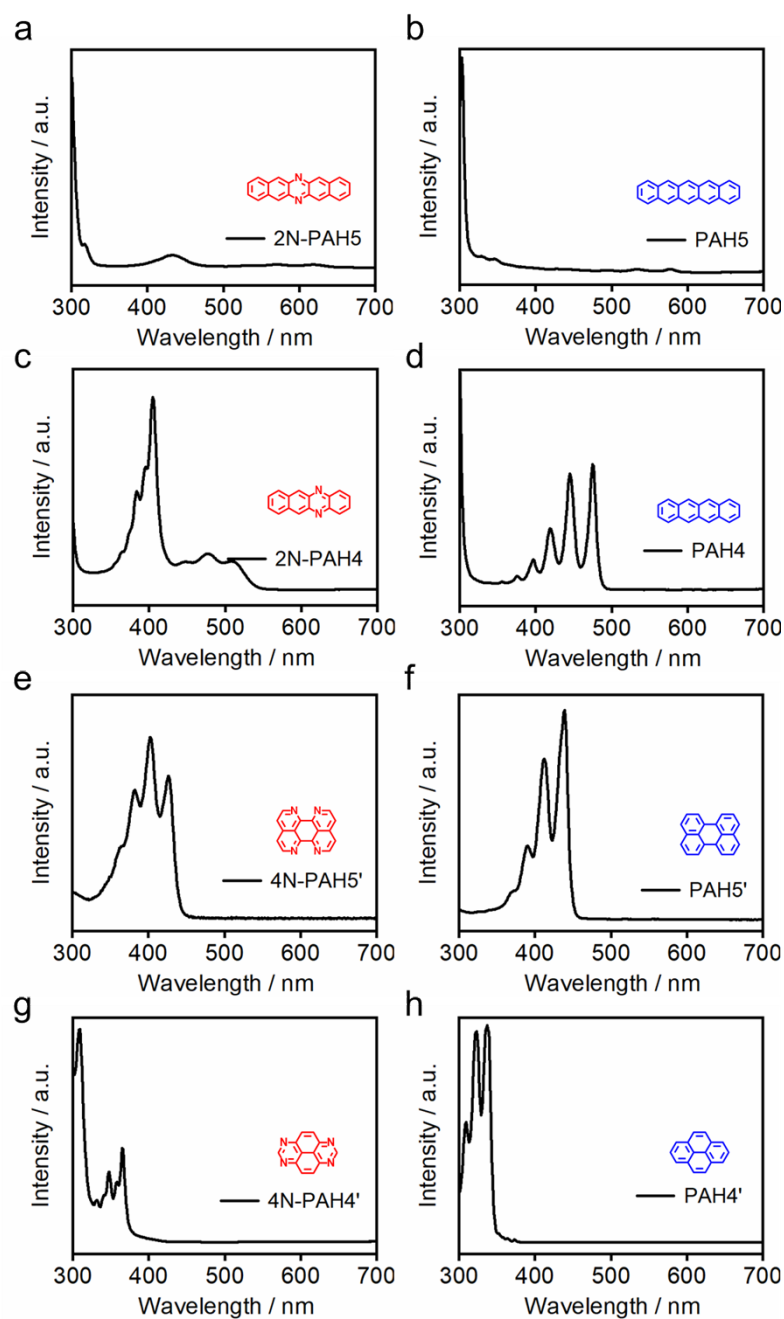


Fig. S7. UV-Vis spectra of 2N-PAH5 (a), PAH5 (b), 2N-PAH4 (c), PAH4 (d), 4N-PAH5' (e), PAH5' (f), 4N-PAH4' (g) and PAH4' (h) in chloroform.

Supplementary Table S3. Energy gap of N-PAHs and PAHs by UV-Vis

N-PAH	2N-PAH5	2N-PAH4	4N-PAH5'	4N-PAH4'
<i>E_g</i> / eV	1.91	2.25	2.71	2.93

PAH	PAH5	PAH4	PAH5'	PAH4'
<i>E_g</i> / eV	2.08	2.51	2.70	3.35

6. Computational methods

The optimized geometry and ground state Hamiltonian and overlap matrix elements of each structure studied in this paper was self-consistently obtained using the SIESTA implementation⁴ of density functional theory (DFT). SIESTA employs norm-conserving pseudo-potentials to account for the core electrons and linear combinations of atomic orbitals to construct the valence states. The generalized gradient approximation (GGA) of the exchange and correlation functional is used with the Perdew-Burke-Ernzerhof parameterization (ca) a double- ζ (DZ) basis set, a real-space grid defined with an equivalent energy cut-off of 150 Ry. The geometry optimization for each structure is performed to the forces smaller than 20 meV/Å.

The mean-field Hamiltonian obtained from the converged DFT calculation was combined with Gollum⁵⁻⁶ implementation of the non-equilibrium Green's function method⁶ to calculate the phase-coherent, elastic scattering properties of each system consist of left graphene (source) and right graphene (drain) leads and the scattering region. The transmission coefficient $T(E)$ for electrons of energy E (passing from the source to the drain) is calculated via the relation:

$$T(E) = \text{Trace} \left(\Gamma_R(E) G^R(E) \Gamma_L(E) G^{R\dagger}(E) \right). \quad \text{In this expression,}$$

$\Gamma_{LR}(E) = i(\Sigma_{LR}(E) - \Sigma_{LR}^\dagger(E))$ describe the level broadening due to the coupling between left (L) and right (R) electrodes and the central scattering region, $\Sigma_{LR}(E)$ are the retarded self-energies associated with this coupling and $G^R = (ES - H - \Sigma_L - \Sigma_R)^{-1}$ is the retarded Green's function.

The electrical conductance is then calculated using the Landauer formula

$$G(E_F, T) = G_0 \int_{-\infty}^{+\infty} dE T(E) \left(-\partial f(E, T, E_F) / \partial E \right), \quad \text{where } f = \left(e^{(E - E_F)/k_B T} + 1 \right)^{-1} \text{ is the}$$

Fermi-Dirac probability distribution function, T is the temperature, E_F is the Fermi energy, $G_0 = 2e^2/h$ is the conductance quantum, e is the electron charge, and h is the Planck's constant.

7. Supplementary computational figures, tables and discussion

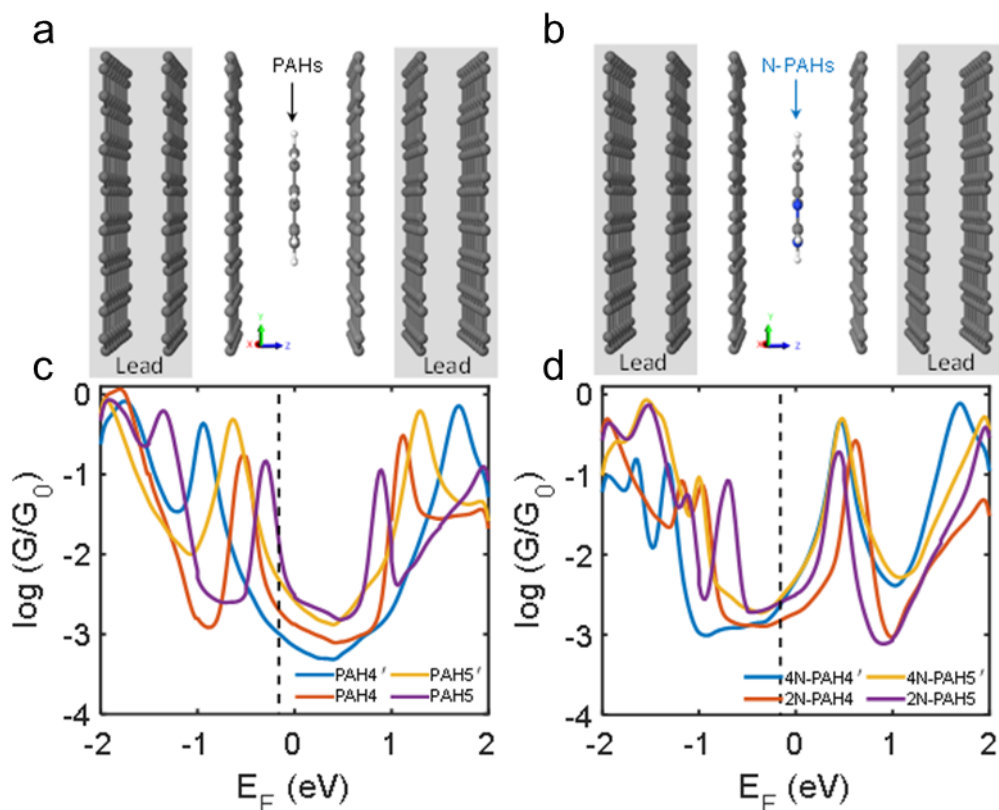


Fig. S8. (a, b) Structure of sandwiched molecular junctions with PAH and N-PAH molecules between two graphene electrodes, respectively. (c, d) Calculated ensemble average conductance of 3 different configurations (from AB to AA stacking) of N-PAH and PAH molecules between graphene electrodes with multiple k -points perpendicular to the z direction.

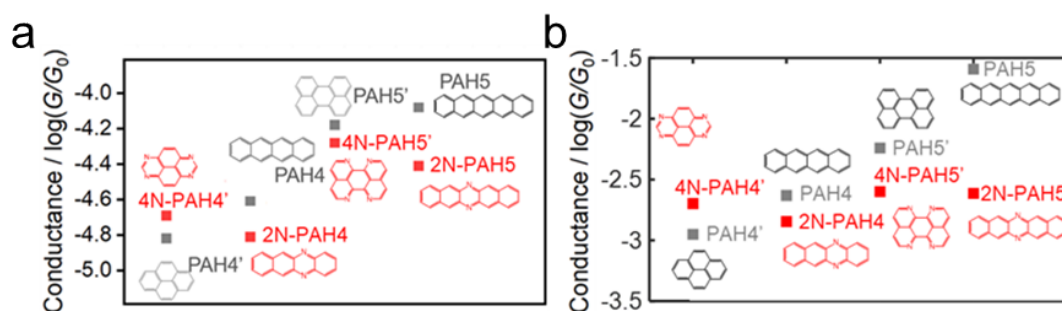


Fig. S9. Measured (a) and calculated (b) electrical conductance of PAHs (gray) and N-PAHs (red), respectively. In (b), calculated ensemble average conductance is obtained at $E_F = 0.18$ eV in Figure S8 (c,d).

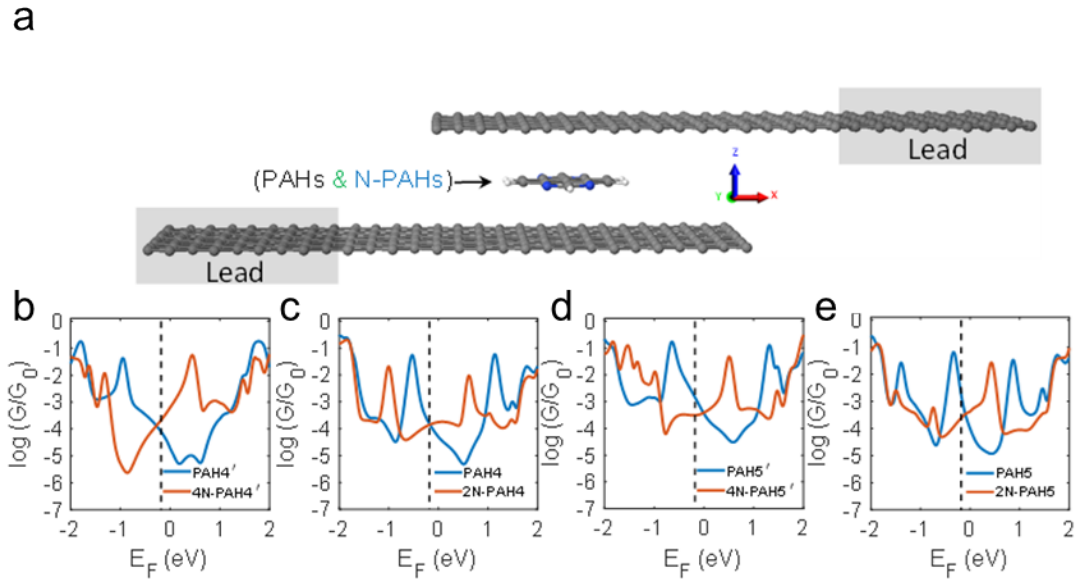


Fig. S10. (a) Structure of sandwiched molecular junctions with PAH and N-PAH molecules between two graphene electrodes. (b, c, d, e) Boltzmann-weighted average conductance of 5 different configurations (from AB to AA stacking) of N-PAH and PAH molecules between graphene electrodes with multiple k -points (20) perpendicular to the z direction.

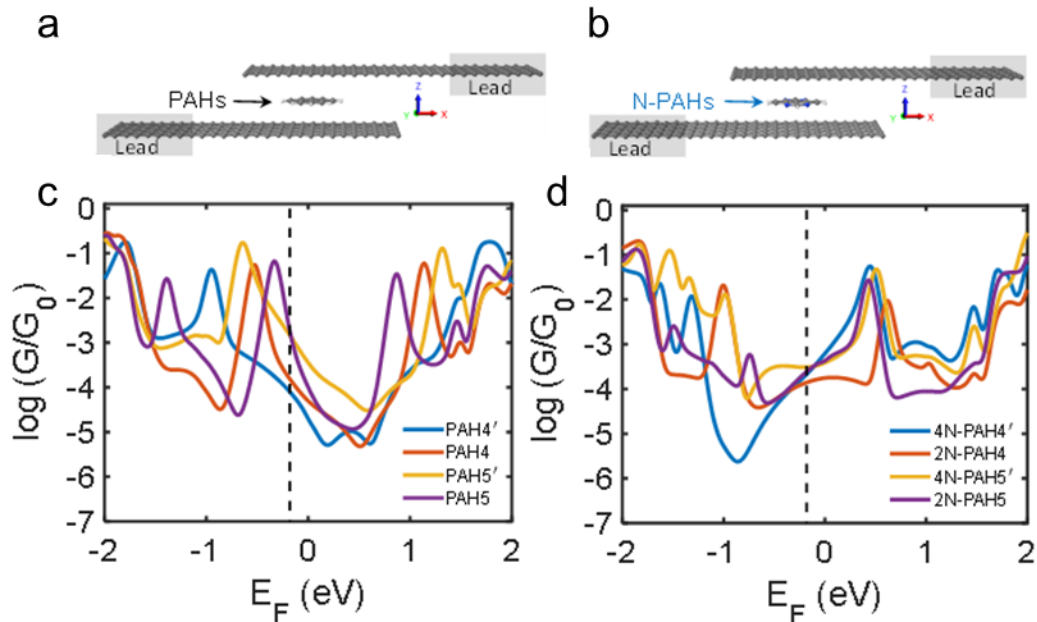


Fig. S11. (a, c) Structure of sandwiched molecular junctions with PAH and N-PAH molecules between two graphene electrodes, respectively. (b, d) Boltzmann-weighted average conductance of 5 different configurations (from AB to AA stacking) of N-PAH and PAH molecules between graphene electrodes with multiple k -points (20) perpendicular to the z direction.

Supplementary Table S4. Frontier orbitals of relaxed structures of PAHs and N-PAHs molecules from HOMO-3 to LUMO+3 orbitals in (eV) energy unit.

Molecule	HOMO-3	HOMO-2	HOMO-1	HOMO	H-L Gap (eV)	LUMO	LUMO+1	LUMO+2	LUMO+3
	 -6.50	 -6.00	 -5.50	 -4.66	2.72	 -1.94	 -1.03	 -0.53	 0.12
	 -6.35	 -6.35	 -5.54	 -5.21	1.75	 -3.46	 -2.17	 -1.46	 -1.21
	 -6.53	 -5.72	 -5.50	 -4.21	1.72	 -2.49	 -0.98	 -0.75	 0.21
	 -6.09	 -5.92	 -4.86	 -4.77	1.67	 -3.10	 -1.34	 -1.12	 -0.24
	 -5.95	 -5.92	 -5.78	 -4.31	2.01	 -2.30	 -0.83	 -0.61	 -0.48
	 -5.37	 -5.32	 -5.10	 -4.73	1.43	 -3.30	 -1.69	 -1.37	 -1.24
	 -6.08	 -5.71	 -5.11	 -3.99	1.23	 -2.76	 -1.46	 -0.79	 -0.31
	 -6.02	 -5.35	 -4.82	 -4.50	1.20	 -3.30	 -1.68	 -1.10	 -0.86

Supplementary Table S5. vdW distance between graphene and molecules in the relaxed ground state configuration

N-PAH	2N-PAH5	2N-PAH4	4N-PAH5'	4N-PAH4'
vdW distance / Å	3.460	3.428	3.425	3.420
PAH	PAH5	PAH4	PAH5'	PAH4'
vdW distance / Å	3.430	3.432	3.460	3.460

8. Gold-based single-molecule junction measurement

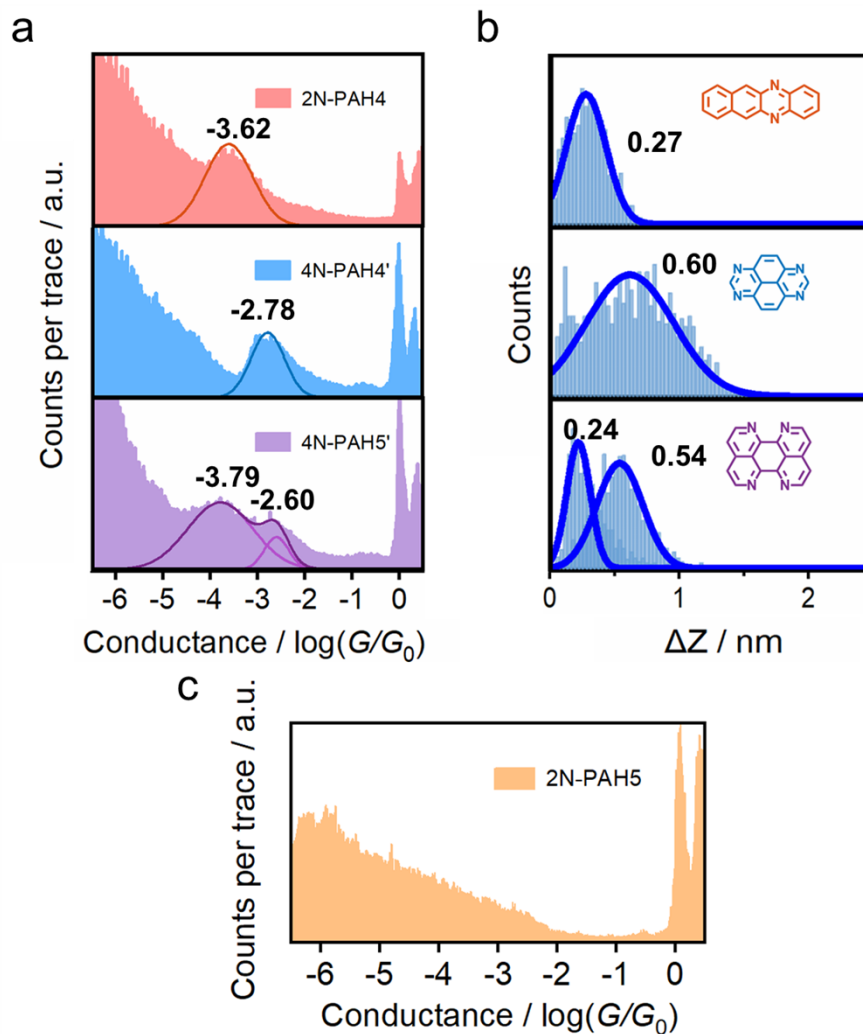


Fig. S12. Electrical properties using gold electrodes with STM-BJ technique at room temperature. (a) 1D conductance histograms obtained from ~ 1000 conductance-displacement traces of 2N-PAH4, 4N-PAH4' and 4N-PAH5'. (b) The plateau length histograms of 2N-PAH4, 4N-PAH4', and 4N-PAH5'. (c) 1D conductance histograms of 2N-PAH5.

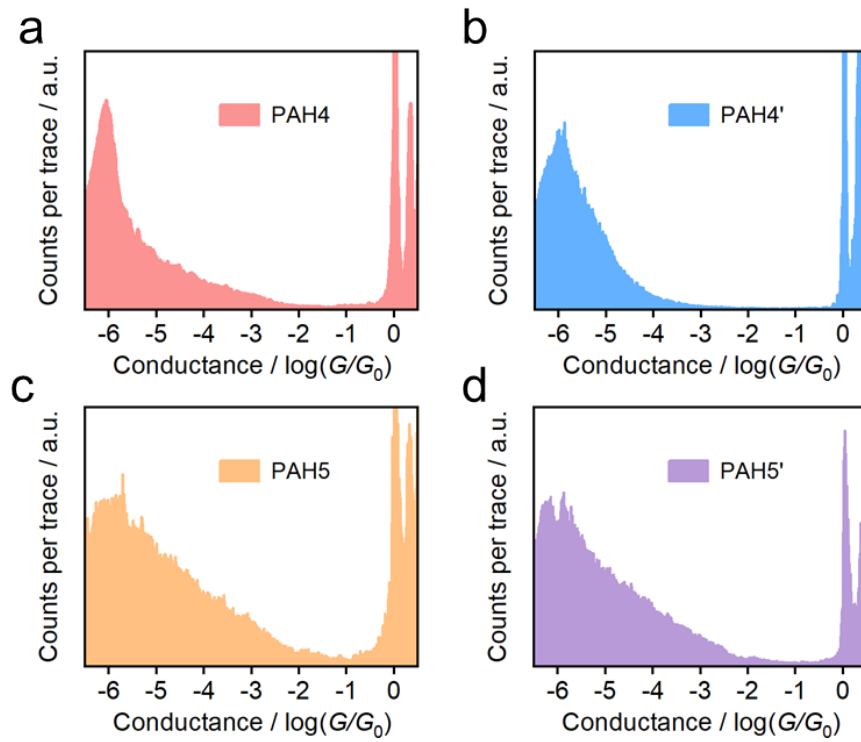


Fig. S13. Electrical properties using gold electrodes with STM-BJ technique at room temperature. 1D conductance histograms of PAH4 (a), PAH4' (b), PAH5 (c), PAH5' (d).

Supplementary references

1. S. Caneva, P. Gehring, V. M. García-Suárez, A. García-Fuente, D. Stefani, I. J. Olavarria-Contreras, J. Ferrer, C. Dekker, H. S. J. van der Zant, *Nat. Nanotechnol.* 2018, **13**, 1126-1131.
2. S. Zhao, Q. Wu, J. Pi, J. Liu, J. Zheng, S. Hou, J. Wei, R. Li, H. Sadeghi, Y. Yang, J. Shi, Z. Chen, Z. Xiao, C. Lambert, W. Hong, *Sci. Adv.* 2020, **6**, eaba6714.
3. S. Zhao, Z.-Y. Deng, S. Albalawi, Q. Wu, L. Chen, H. Zhang, X.-J. Zhao, H. Hou, S. Hou, G. Dong, Y. Yang, J. Shi, C. Lambert, Y.-Z. Tan, W. Hong, *Chem. Sci.* 2022, **13**, 5854-5859.
4. J. M. Soler, E. Artacho, J. D. Gale, A. García, J. Junquera, P. Ordejón, D. Sánchez-Portal, *J. Phys. Condens* 2002, **14**, 2745-2779.
5. J. Ferrer, C. J. Lambert, V. M. García-Suárez, D. Z. Manrique, D. Visontai, L. Oroszlany, R. Rodríguez-Ferradás, I. Grace, S. W. D. Bailey, K. Gillemot, H. Sadeghi, L. A. Algharagholy, *New J. Phys.* 2014, **16**, 093029.
6. H. Sadeghi, *Nanotechnology* 2018, **29**, 373001.